RSC Advances

PAPER

View Article Online
View Journal | View Issue

Check for updates

Cite this: *RSC Adv.*, 2020, **10**, 6547

Corrosion inhibition on mild steel in 1 M HCl solution by *Cryptocarya nigra* extracts and three of its constituents (alkaloids)

Mas Faiz,[a] Azeana Zahari,*[a] Khalijah Awang[a] and Hazwan Hussin[b]

Corrosion inhibition effect of the crude extracts (hexane, dichloromethane, methanol) from the bark of *Cryptocarya nigra* and three alkaloids named *N*-methylisococlaurine **1**, *N*-methyllaurotetanine **2** and atherosperminine **3** isolated from the *Cryptocarya nigra* dichloromethane extract (CNDE) were investigated for mild steel corrosion in 1 M HCl solution. An electrochemical impedance study showed that CNDE and **2** reduced the corrosion significantly through a charge transfer mechanism with inhibition efficiency of 91.05% and 88.05%, respectively. Potentiodynamic polarization data indicated that CNDE acted through anodic type inhibition while **2** was a mixed type inhibitor with predominant anodic effectiveness. ΔG_{ads} values calculated from the Langmuir adsorption isotherm plots for CNDE (−28.2 kJ mol^{-1}) and **2** (−13.2 kJ mol^{-1}) suggested that they adsorbed on the mild steel surface *via* a physisorption mechanism. Scanning electron microscopy micrographs and elemental composition studies confirmed the formation of a protective film over the metal surface. Wastewater quality parameters of all the inhibitors demonstrated good biodegradability as their values were within the permissible limits to discharge for irrigation and horticultural uses.

Received 22nd July 2019
Accepted 16th January 2020

DOI: 10.1039/c9ra05654h

rsc.li/rsc-advances

Open Access Article. Published on 12 February 2020. Downloaded on 1/23/2026 3:02:15 PM.
This article is licensed under a Creative Commons Attribution-NonCommercial 3.0 Unported Licence.

1. Introduction

Corrosion is the deterioration of a metal surface due to, in many cases, unavoidable slow continuous oxidation and reduction reactions. An average cost of $2.5 trillion, approximately 3.4% of the world's domestic product annually worldwide suffered from the impact of corrosion according to a study done by NACE International.[1] Therefore, the prevention of this undesired phenomenon could be a practical solution to investigate this problem. Acidic media which are widely used in industrial acid cleaning, acid descaling, and acid pickling require the use of corrosion inhibitors to restrain corrosion on metallic materials.[2] The synthetic organic and inorganic corrosion inhibitors are effective but are harmful to humans and the environment. Hence, the study of corrosion prevention particularly on mild steel using plant-based corrosion inhibitors is of tremendous interest as plant extracts are found in abundance, inexpensive, less or nontoxic, biodegradable and biocompatible.[3] Over the years, considerable efforts have been focused in finding suitable green corrosion inhibitors of organic origin such as tea leaves,[4] *Hibiscus sabdariffa*,[5] *Musa paradisiaca*,[6] *Justicia gendarussa*,[7] *Uncaria gambir*,[8] *Rollinia occidentalis*,[9] *Glycyrrhia glabra* extract,[10] *Citrus aurantifolia*,[11] *Neolamarckia cadamba*,[12] and *Rhizophora apiculate*.[13] The most important feature of an extract to behave as an efficient acid inhibitor is to contain organic compounds with oxygen, nitrogen, sulphur and/or phosphorus in their structures as described by Chigondo *et al.*[14] and Verma *et al.*[2] in their recent review articles. Their extent of inhibition depends on the effective organic groups attached and increases in the order: oxygen < nitrogen < sulphur < phosphorus. Several compounds possessing heteroatoms that have been reported to exert anti-corrosive activities are 3β-isodihydrocadambine,[12] perakine, tetrahydroalstonine,[15] and isoreserpiline.[16]

Malaysian flora is known to be one of the richest forest ecosystems in the world with at least 15 000 documented plant species.[17] Therefore, it is a strategic region to search for plausible natural corrosion inhibitors. Among the prevalent species available, *Cryptocarya nigra* was specifically selected for this work due to its capacity to yield many types of interesting chemical constituents containing heteroatoms such as nitrogen and oxygen.[18] This plant is widely distributed in Sumatra and Borneo and it is locally known in Peninsular Malaysia as 'Medang'. Only 19 species from the genus *Cryptocarya* which belonged to the family Lauraceae are found in Malaysia.[19] A survey of the literature on phytochemical and pharmacological studies, *Cryptocarya* has been a prolific producer of flavonoids, chalcones, lactones, α-pyrones and alkaloids.[17,18] Anti-plasmodial, anti-oxidant, anti-cholinesterase, anti-bacterial and cytotoxicity[20] activity studies particularly on alkaloids have been published from this species. However, to date, no

[a]*Department of Chemistry, Faculty of Science, University of Malaya, 50603 Kuala Lumpur, Malaysia. E-mail: azeanazahari@um.edu.my; Fax: +60-79674193; Tel: +60-79674064*

[b]*Materials Technology Research Group (MaTReC), School of Chemical Sciences, Universiti Sains Malaysia, 11800 Minden, Penang, Malaysia*

Open Access Article. Published on 12 February 2020. Downloaded on 1/23/2026 3:02:15 PM.
This article is licensed under a Creative Commons Attribution-NonCommercial 3.0 Unported Licence.

work on *Cryptocarya* as a potential source of corrosion inhibitor has been reported. This research has been inspired by the fact that anti-oxidant secondary metabolites containing polyphenolic groups such as alkaloids may assist in the protection of metal towards corrosion.[21]

In view of the above together with our continuing efforts in searching for eco-friendly plant-based compounds for industrial use,[12,16] our group has investigated corrosion inhibition properties of *Cryptocarya nigra* for the first time. This paper reports the results of corrosion inhibition study of the *Cryptocarya nigra* bark crude extracts (hexane, dichloromethane, methanol) and three known alkaloids; *N*-methylisococlaurine **1**, *N*-methyllaurotetanine **2** and atherosperminine **3**, isolated from the dichloromethane extract.

2. Experimental

The bark of *Cryptocarya nigra* was collected at Hutan Simpan Ulu Sat, Machang, Kelantan (Malaysia) by Mr Teo, Mr Rafly and Mr Din from the phytochemical group before being deposited at the Herbarium of the Department of Chemistry, University of Malaya, Kuala Lumpur, Malaysia for research reservations. The voucher specimen was given code number KL 5272.

2.1 Extraction and isolation

The air-dried ground bark of the plant (2.5 kg) was first defatted with hexane (15 L) by cold percolation at room temperature for 3 days repeatedly. The crude was combined and evaporated to give 4.7 g of hexane extract designated as CNHE. The dried plant material was made alkaline and moistened with 25% NH_4OH (100 mL) for 4 hours to aggregate the nitrogen-containing components. It was then macerated with CH_2Cl_2 (15 L) 3 times for a 3 day period. The supernatant was finally concentrated and dried to give 13.2 g of *Cryptocarya nigra* dichloromethane extract (CNDE). The residues were soaked again with MeOH (15 L) for a period of 3 days at room temperature to obtain 8.95 g of *Cryptocarya nigra* methanol extract (CNME). All the crude extracts were each obtained in the form of sticky dark brown residues.

8.0 g of CNDE was subjected to column chromatography over silica gel using CH_2Cl_2 and MeOH solvent systems (100 : 0, 99 : 1, 98 : 2, 97 : 3, 96 : 4, 95 : 5, 94 : 6, 90 : 10, 85 : 25, 75 : 25, 50 : 50) and finally 100% methanol as eluent to obtain 300 fractions. The alkaloid spots were first detected by UV light (254 and 365 nm) and confirmed by spraying with Dragendorff's reagent. Orange stains having the same R_f values were combined and treated as a group. Further purification of fractions 130, 110 and 90 by Preparative Thin Layer Chromatography (PTLC) yielded **1** (23.0 mg, MeOH–CH_2Cl_2; 95 : 5: saturated with NH_4OH), **2** (18.0 mg, MeOH–CH_2Cl_2; 96 : 4: saturated with NH_4OH), and **3** (18.0 mg, MeOH–CH_2Cl_2; 96 : 4: saturated with NH_4OH), respectively. The structures of the isolated alkaloids were elucidated with the aid of various complementary spectroscopic methods such as 1D-NMR (^1H, ^{13}C and DEPT), 2D-NMR (COSY, NOESY, HSQC and HMBC), FTIR and LCMS-IT-TOF, in comparison with the literature values.

2.2 Characterization of the alkaloids

The 1D and 2D NMR spectra were acquired using Bruker AVN 400 FT NMR spectrometer system and analyzed *via* the TopSpin software package. LCMS-IT-TOF was performed using Agilent Technologies 6530 Accurate-Mass Q-TOF LC/MS, with ZORBAX Eclipse XDB-C18 Rapid Resolution HT 4.6 mm i.d. × 50 mm × 1.8 μm column. HPLC grade methanol, acetonitrile and deionized water were used as mobile phase solvents. IR absorption bands were recorded using a PerkinElmer Spectrum 400 FT-IR spectrometer.

2.3 Corrosion inhibition study

Mild steel (MS) specimens with standard compositions scanned under X-ray fluorescence (XRF) were used during this experiment. MS with an exposed area of 3.142 cm^2 and 2 × 0.2 × 3 cm was applied for the electrochemical and SEM analysis, respectively. Their surfaces were abraded with sandpapers, degreased with acetone and cleansed with distilled water before performing each of the electrochemical experiments. 37% HCl was diluted into 1 M HCl in a 1 L volumetric flask as the stock solution. The stock solution was then combined with different concentrations of inhibitors to prepare electrolytes ranging from 10, 100, 200, 500 and 1000 mg L^{-1}, denoted as ppm.

Gamry Instruments reference 600 (potentiostat/galvanostat/ZRA) is the instrument used to perform the electrochemical analysis. It is a conventional three-electrode system that can contain approximately 50 mL of electrolyte. MS specimens were

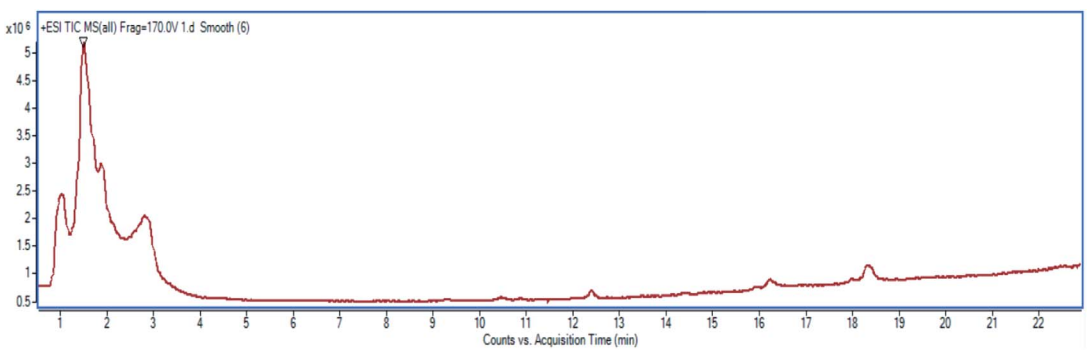

Fig. 1 Refined LC profile spectra under positive mode (+1).

 This journal is © The Royal Society of Chemistry 2020

Open Access Article. Published on 12 February 2020. Downloaded on 1/23/2026 3:02:15 PM.
This article is licensed under a Creative Commons Attribution-NonCommercial 3.0 Unported Licence.

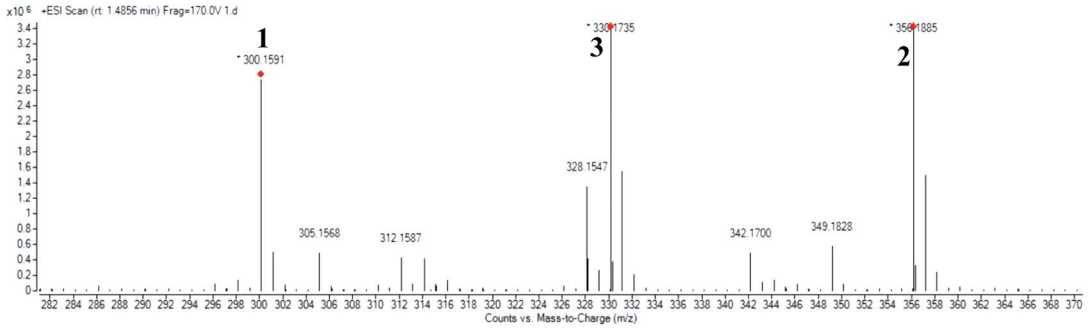

Fig. 2 Molecular mass fragmentations at $R_t = 1.4856$.

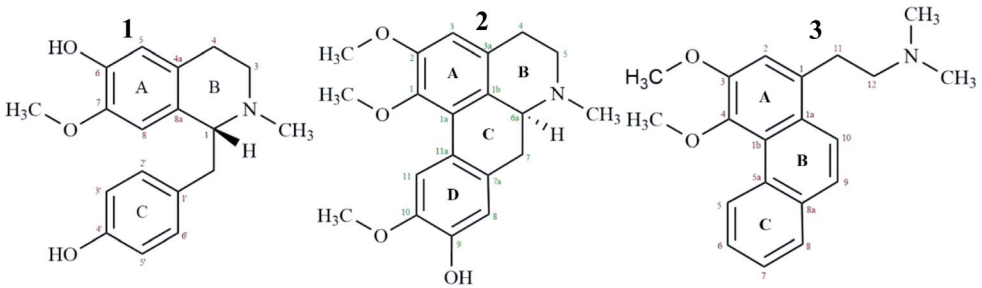

Fig. 3 Alkaloids isolated from CNDE tested for corrosion inhibition study.

placed as the working electrode, while platinum (Pt) as the auxiliary electrode and saturated calomel electrode (SCE) as the reference electrodes, respectively. A steady-state open circuit potential, E_{ocp} was attained upon immersion of the working electrode in the test solution for 30 minutes with a signal amplitude perturbation of 5 mV. The fitting of the impedance data to an equivalent electrical impedance circuit was accomplished by using the GAMRY Echem Analyst software package 5.50. It was also used to extrapolate the Tafel slopes from the potentiodynamic polarization experiment.

2.3.1 Electrochemical impedance study (EIS). Alternate Current (AC) impedance measurements were done at a potential amplitude of 10 mV, peak-to-peak in an open circuit with 10 points per decade and the frequency ranging from 0.1 to 10 000 Hz. The impedance results obtained were represented as Nyquist plots. The following eqn (1) is used to calculate the inhibition efficiency (IE%):[8]

$$\mathrm{IE}(\%) = \left(1 - \frac{R_{ct(0)}}{R_{ct(i)}}\right) \times 100 \quad (1)$$

where $R_{ct(0)}$ is the charge transfer resistance of MS without inhibitor, $R_{ct(i)}$ is the charge transfer resistance of MS with inhibitor.

2.3.2 Potentiodynamic polarization study (PDP). The working electrode was scanned from −800 mV to −200 mV (*vs.* SCE) with a scan rate of 0.5 mV s^{-1}. The linear Tafel tangent was chosen approximately 10–40 mV from the corrosion potential, E_{corr}, of the anodic and cathodic curves. Corrosion current density (i_{corr}) were obtained from the extrapolation of the points to E_{corr}. Eqn (2) below shows the calculation of IE (%) from the i_{corr} values:[21]

$$\mathrm{IE}(\%) = \left(1 - \frac{i_{corr(i)}}{i_{corr(0)}}\right) \times 100 \quad (2)$$

where $i_{corr(0)}$ is the corrosion current density of MS without inhibitor, $i_{corr(i)}$ is the corrosion current density of MS with inhibitor.

2.4 Characteristic, analytic and sampling of wastewater

The purpose of this experiment is to provide supporting information on the biodegradability of the pure compounds in consideration of practical application as green corrosion inhibitors for the industry. In this paper, the quality of wastewater produced was evaluated as a function of four effluent quality parameters namely; (i) chemical oxygen demand (COD), (ii) biochemical oxygen demand (BOD), (iii) metal content and (iv) pH. The testing was conducted according to the methods

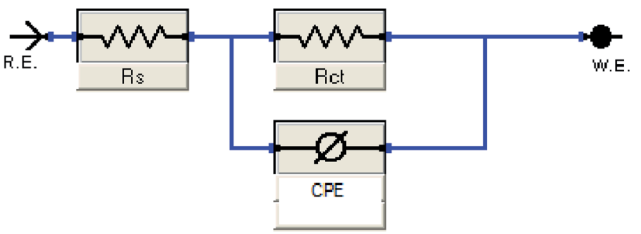

Fig. 4 The Randle's CPE equivalent circuit used to fit the impedance data.

Open Access Article. Published on 12 February 2020. Downloaded on 1/23/2026 3:02:15 PM.
This article is licensed under a Creative Commons Attribution-NonCommercial 3.0 Unported Licence.

prescribed in APHA (American Public Health Association, 1989) handbook at the wastewater treatment lab of TopGlove International Sdn. Bhd. R&D centre, Malaysia.

2.4.1 Determination of BOD. This method measures the total organic substances that could be metabolized by the act of natural microorganism present in the body of receiving water samples. The Hach WIMS BOD Manager utilizes the following calculations to perform the BOD experiment. 10 mg of each inhibitor sample was prepared and diluted into a 300 mL BOD bottle containing aerated deionized water. The initial dissolved oxygen (DO) value was measured by probe, stored at 20 °C, continuously aerated and adjusted to pH 7 before test. After the incubation period of five days, final DO was taken. The difference between the final and initial DO reading was computed using eqn (3) and represents the BOD of the sample.

$$\text{BOD}\ \ (\text{mg L}^{-1}) = \frac{\left[\text{DO}_{\text{initial}} - \text{DO}_{\text{final}}\right]\ \text{mg L}^{-1}}{\text{vol}_{\text{sample}}\ (\text{mL})} \times \text{vol}_{\text{bottle}}\ (\text{mL}) \tag{3}$$

The samples should be kept below 4 °C to prevent any undesired changes incur and testing should be carried out as quickly as possible. Do not allow samples to freeze. They may be kept for not longer than 48 hours before beginning the BOD test.[22]

2.4.2 Determination of COD. The disadvantages of the BOD test have led to the development of a simpler and quicker test. This test is known as the chemical oxygen demand (COD) methodology. In this test, strong chemical reagents are used to oxidise the waste. Potassium dichromate is used in conjunction with boiling concentrated sulphuric acid and a silver catalyst. The waste is refluxed in this mixture for two hours. The consumption of the chemical oxidant can be related to the corresponding oxygen demand. The COD test oxidises material that micro-organisms cannot metabolise in five days or that are toxic. If the COD $\gg$ BOD in raw wastewater, then the waste is not readily biodegradable, and may be toxic to the micro-organism. If COD $\approx$ BOD, then the waste is readily biodegradable.[22]

This experiment measures the total organic and inorganic material that could be oxidized in the tested wastewater samples by using dichromate in 50% sulphuric acid, H_2SO_4. In this experiment, 20 mL of the aerated solution was transferred into the determining bottle of COD measurement system. They were incubated homogenously at 20 °C with the aid of magnetic stirring. The biodegradation extent of wastewater was expressed as oxygen consumption *versus* original COD. At between time intervals, 5 mL of wastewater was sampled for COD and BOD determination.

3. Results and discussions

The structural elucidation, corrosion inhibition and biodegradability of the studied inhibitors are described in this section.

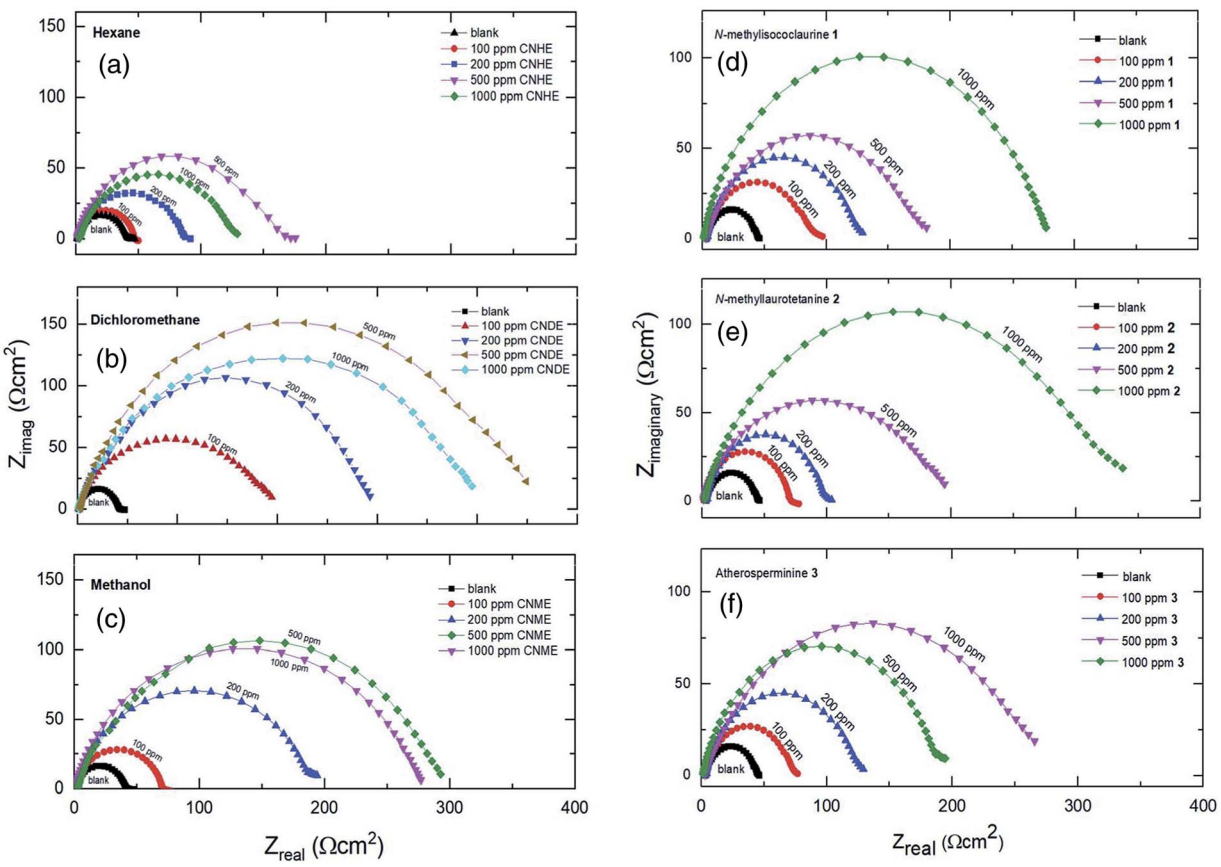

Fig. 5 Nyquist plots for all concentrations of inhibitors in 1 M HCl at 303 K.

 This journal is © The Royal Society of Chemistry 2020

Open Access Article. Published on 12 February 2020. Downloaded on 1/23/2026 3:02:15 PM.
This article is licensed under a Creative Commons Attribution-NonCommercial 3.0 Unported Licence.

3.1 Compounds identification and characterization

High resolution liquid chromatography-ion trap-time of flight mass spectrometry (LCMS-IT-TOF) was used to obtain the LCMS profile of CNDE before further purification steps were done. The refined LC profile spectra under positive mode (+1) and molecular mass fragmentation at retention time $R_t = 1.4856$ of CNDE are depicted in Fig. 1 and 2, respectively. The presence of **1**, **2** and **3** were observed from the mass values (m/z) 300.1591, 342.1699 and 310.1802 respectively. **1** is a benzyl isoquinoline with 2 hydroxyl and 1 methoxyl group. **2** is an aporphine with 1 hydroxyl and 3 methoxyl groups. **3** is a phenanthrene with only 2 methoxyl groups (Fig. 3). It is worthy to take note that alkaloids have nitrogen (N) as the base element in their structures. The N atom can serve as a protonating site for H^+ and binds onto the steel surface through physisorption or act as a nucleophilic site to form coordinative bonds towards the vacant low energy orbitals of the steel surface.[23]

3.1.1 *N*-Methylisococlaurine 1. Brownish amorphous solid; $[\alpha_D^{25}] = +52.5$ ($c = 1.0$, MeOH); IR (KBr) $\nu_{max} = 3583, 2921, 2852, 2357, 1738, 1600, 1444, 1258, 1110$ cm^{-1}. LCMS-IT-TOF gave a pseudo-molecular ion peak at m/z 300.1593 calculated for $C_{18}H_{21}NO_3$ $(M + H)^+$. ^{1}H NMR (400 MHz, $CDCl_3$) δ: 6.89 (2H, d, $J = 8.5$, H-6′/2′), 6.58 (2H, d, $J = 8.5$, H-3′/5′), 6.47 (1H, s, H-5), 6.31 (1H, s, H-8), 3.78 (3H, s, 7 OMe), 3.64 (1H, t, $J = 6.5$, H-1), 3.17–3.11 (1H, m, H-3a), 3.00 (1H, dd, $J_g = 12.4$ Hz, $J_v = 6.8$ Hz, H-α_a), 2.79–2.78 (2H, dd, $J_v = 6.2$, $J_g = 13$ Hz, H-3b & H-4a), 2.74–2.71 (1H, m, α_b), 2.54–2.50 (1H, m, H-4b), 2.42 (3H, s, *N*-Me). ^{13}C NMR (400 MHz, $CDCl_3$) δ: 154 (C-4′), 145 (C-6), 143 (C-7), 131 (C-1′), 130.4 (C-2′/6′), 130.1 (C-8a), 125 (C-4a), 115 (C-3′/5′), 114 (C-8), 110 (C-5), 64 (C-1), 56 (C-7 OMe), 44 (C-3), 42 (C-*N*Me), 40 (C-α), 24 (C-4).[24,25]

3.1.2 *N*-Methyllaurotetanine 2. Dark brownish amorphous solid; $[\alpha_D^{25}] = +75.0$ ($c = 1.0$, MeOH); IR (KBr) $\nu_{max} = 3480, 2920, 2962, 2352, 1728, 1512, 1223, 1157, 1028$ cm^{-1}. LCMS-IT-TOF gave a pseudo-molecular ion peak at m/z 342.1854 $(M + H)^+$. ^{1}H NMR (400 MHz, $CDCl_3$) δ: 7.98 (1H, s, H-11), 6.83 (1H, s, H-8), 6.81 (1H, s, H-3), 3.86 (3H, s, 10-OMe), 3.88 (3H, s, 2-OMe), 3.67 (3H, s, 1-OMe), 3.19 (1H, m, H-4b), 3.04 (1H, m, H-5b), 3.00 (1H, m, H-6a), 2.96 (1H, m, H-7b) 2.68 (1H, m, H-4a), 2.64 (1H, m, H-5a), 2.54 (3H, s, *N*-Me), 2.38 (1H, m, H-7b). ^{13}C NMR (400 MHz, $CDCl_3$) δ: 152 (C-2), 145.4 (C-10), 145 (C-9), 144 (C-1), 130 (C-7a), 127 (C-1a), 127 (C-3a), 123.9 (C-11a), 123 (C-1b), 114 (C-8), 111 (C-11), 110 (C-3), 62 (C-6a), 60 (1-C-OMe), 56 (10-C-OMe), 55 (2-C-OMe), 53 (C-5), 44 (*N*-Me), 34 (C-7), 30 (C-4).[26,27]

3.1.3 Atherosperminine 3. Yellowish amorphous solid; $[\alpha_D^{25}] = +15.0$ ($c = 1.0$, MeOH); IR (KBr) $\nu_{max} = 2917, 2849, 1706, 1646, 1604, 1512, 1463, 1223, 1129$ cm^{-1}. LCMS-IT-TOF gave a pseudo-molecular ion peak at m/z 310.1802 $(M + H)^+$. ^{1}H NMR (400 MHz, $CDCl_3$) δ: 9.68 (1H, d, $J = 8.32$, H-5), 7.88 (1H, dd, $J_o = 9.04$, $J_m = 2.8$ Hz, H-8), 7.60–7.58 (3H, m, H-6/7/9), 7.26 (1H, s, H-2), 4.06 (3H, s, 3-OMe), 3.94 (3H, s, 4-OMe), 3.33 (2H, m, H-11), 2.70 (2H, m, H-12), 2.44 (–*N*(Me)$_2$). ^{13}C NMR (400 MHz, $CDCl_3$) δ: 150.8 (C-3), 145 (C-4), 133 (C-8a), 132 (C-5a), 130 (C-1), 128.1 (C-5/8), 126.6 (C-9), 126.5 (C-6), 126.1 (C-1a), 125.7 (C-7), 125.2 (C-1b), 122.5 (C-10), 114 (C-2), 60.0 (C-12), 59.9 (4-C-OMe), 56.6 (3-C-OMe), 45.4 (–*N*(Me)$_2$), 32.4 (C-11).[28]

3.2 Corrosion inhibition study

The open-circuit potential, E_{ocp} for each of the experiments conducted was first examined for 10 minutes before applying electrochemical impedance study (EIS) to obtain a steady current reading on the mild steel surface.

3.2.1 Electrochemical impedance study (EIS). This study was performed to investigate the amount of current flow and the resistance value occurring on the MS surface with and without the presence of inhibitors. All the processes involved in the electrical response of the system were fitted against an equivalent Randle CPE circuit model, Fig. 4 and illustrated as Nyquist plots, Fig. 5. Solution resistance (R_s) describes the ohmic resistance while the charge transfer resistance (R_{ct}) represents the inhibitor's resistance towards oxidation of the metal surface and it is inversely proportional to the corrosion rate. Pure double layer capacitor (C_{dl}) is replaced by a constant phase element (CPE) to justify the semicircle shape of the Nyquist plot.[29] The higher the diameter of the Nyquist plot, the higher the R_{ct} value, hence the higher the inhibition efficiency of a given inhibitor.

Based on Table 1, CNDE showed 91.05% of inhibition performance at 500 ppm which is the highest compared to CNHE and CNME. The Nyquist plot for CNDE is depicted in Fig. 5(b). It could be observed that the diameter of Nyquist plots increased upon increasing inhibitors concentration. This could

Table 1 Impedance parameters for all the studied inhibitors on MS in 1 M HCl medium

Inhibitor	Conc. (ppm)	R_s (Ω)	R_{ct} (Ω)	n	CPE (μF cm^{-2})	IE (%)
—	0	1.345	40.53	0.9550	939.8	—
CNHE	10	2.997	42.11	0.7552	822.50	3.75
	100	2.228	54.82	0.6235	735.40	26.06
	200	2.115	66.82	0.7070	722.16	39.34
	500	2.445	85.34	0.7100	601.45	52.50
	1000	2.205	83.70	0.6485	630.42	51.57
CNDE	10	2.299	114.6	0.7480	785.12	64.63
	100	2.682	201.7	0.8422	528.68	79.09
	200	2.107	296.5	0.8826	415.54	86.33
	500	2.702	453.0	0.8248	249.73	**91.05**
	1000	2.737	400.0	0.8375	360.80	89.86
CNME	10	2.228	58.38	0.8602	810.57	30.57
	100	2.238	188.60	0.8522	659.27	78.51
	200	2.150	268.12	0.7562	509.21	84.88
	500	2.680	326.50	0.9210	454.83	87.58
	1000	2.465	301.20	0.8960	472.60	86.54
1	100	2.895	86.2	0.741	628.4	52.98
	200	2.924	129.3	0.792	534.05	68.65
	500	2.735	181.7	0.874	412.6	77.70
	1000	2.697	277.5	0.890	258.4	85.40
2	100	2.740	77.8	0.810	623.6	47.90
	200	2.723	104.3	0.594	600.5	61.14
	500	2.682	195.6	0.599	496.3	79.27
	1000	2.056	338.7	0.602	188.4	**88.05**
3	100	2.890	77.1	0.543	771.2	47.46
	200	2.772	129.4	0.768	569.4	68.67
	500	2.769	184.7	0.681	395.4	78.05
	1000	2.766	268.6	0.630	265.3	82.91

Open Access Article. Published on 12 February 2020. Downloaded on 1/23/2026 3:02:15 PM.
This article is licensed under a Creative Commons Attribution-NonCommercial 3.0 Unported Licence.

correspond to the strengthening of the inhibitive film on mild steel surface.[30] From the ohmic law where $V = IR$, the higher the resistance value (R_{ct}), the lower the electrical current (I) flow, hence, lower number of electrons being transferred across the metal surface. Thus, suggesting that the metal dissolution process (oxidation of iron) was being inhibited.[31] The inhomogeneity of the metal surface resulted in lower values of n ($0.5 < n < 1$; depressed semicircle capacitive loop). The maintained semicircle shapes of the Nyquist plots over the experiments indicated that the corrosion inhibition process occurs through a charge transfer mechanism.[32] CNDE acted as concentration independent inhibitor with low optimum concentration value of 500 ppm as compared to the pure alkaloids. This is because CNDE is made up of several compounds and has indirectly formed a bulkier solution. Above 500 ppm, CNDE showed less IE%. This is because the inhibitors were replaced by water molecules or chloride ions (Cl^-) when the solution is above its critical concentration.[12,33]

On the other hand, the pure alkaloids displayed concentration dependent inhibition patterns with increasing IE% up until 1000 ppm as they have not reached their optimum concentrations. They have higher saturation points above 1000 ppm as compared to their extract (CNDE) due to the less bulk solution formed individually by them.[34] Table 1 revealed that **2** showed 88.05% of inhibition performance at 1000 ppm which was the highest compared to **1** and **3**. The Nyquist plots for each of the alkaloids are shown in Fig. 5(d)–(f). The increase in R_{ct} and decrease in CPE values upon addition of **2** indicated reduction in the corrosion rate with the formation of adsorbed protective film on the metal-solution interface.[35] The inhibition action suppresses both the CPE and corrosion current density (i_{corr}) by replacing water molecules present on the working electrode surface by the inhibitors.[35] The corrosion process was mainly controlled by charge transfer mechanism and the process was characterized by a single relaxation time constant. No change in inhibition mechanism was observed throughout the whole test period upon addition of the alkaloids.[31,36] In a nutshell, all alkaloidal inhibitor solutions showed less R_{ct} values than that of their parent extract, CNDE. The presence of many other constituents in the extract itself may have synergistically improve its corrosion inhibition efficiency simultaneously strengthening the adsorption of crude extracts over the MS surface.[16,37] No change in inhibition mechanism was observed throughout the whole test period upon addition of the alkaloids.[7]

In a nutshell, all alkaloidal inhibitor solutions showed less R_{ct} values than that of their parent extract, CNDE. The presence of many other constituents in the extract itself may have synergistically improve its corrosion inhibition efficiency simultaneously strengthening the adsorption of crude extracts over the MS surface.[32–38]

3.2.2 Potentiodynamic polarization study (PDP). This experiment was carried out to gain knowledge on the reaction

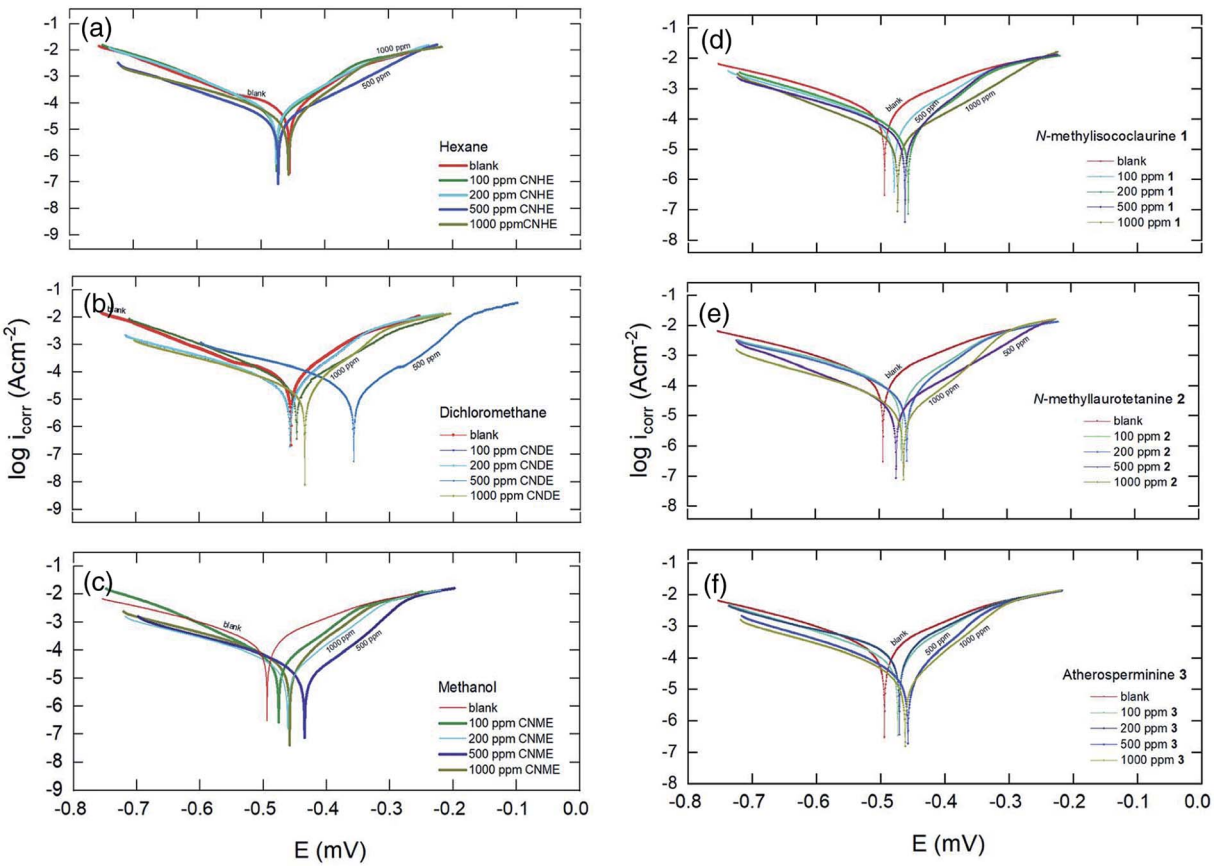

Fig. 6 Nyquist plots for all concentrations of inhibitors in 1 M HCl at 303 K.

 This journal is © The Royal Society of Chemistry 2020

Open Access Article. Published on 12 February 2020. Downloaded on 1/23/2026 3:02:15 PM.
This article is licensed under a Creative Commons Attribution-NonCommercial 3.0 Unported Licence.

kinetics and the type of corrosion inhibition action of the studied inhibitors on the MS surface. Only one anodic (metal dissolution reaction) and two cathodic (hydrogen evolution and dissolved oxygen reduction) are expected in an aerated acidic solution.[39] The obtained polarization curves for MS in 1 M HCl in the absence and presence of different concentrations of inhibitors are shown in Fig. 6. Gradient lines at the cathodic and anodic overpotentials of the experimental Tafel plots were extrapolated by using Gamry Echem Analyst software version 5.50. The results obtained for the IE% of the inhibitors using PDP technique were in close agreement with those obtained using the EIS technique.

From Table 2, CNDE showed 82.64% of IE% at the concentration of 500 ppm which was the highest as compared to CNHE and CNME. Fig. 6(b) displayed the Tafel curves before and after the introduction of various concentrations of CNDE. The E_{corr} values were shifted (±40–100 mV) majorly in the anodic direction simultaneously causing the anodic Tafel slope (β_a) to increase, while the value of cathodic Tafel slopes (β_c) to remain constant confirming that only metal dissolution reaction was reduced by surface blocking effect of the inhibitor.[40] Furthermore, the addition of CNDE reduced the values of current density (i_{corr}) while decreasing the polarization resistance (R_p) which eventually led to the reduction in corrosion rate (CR).[41]

The inhibitive actions of all the alkaloids were concentration dependent up until 1000 ppm and resulted in a marked shift in both cathodic and anodic branches of the Tafel plots. The change in the corrosion potential, E_{corr} remained in between $\Delta E = \pm 1$–30 mV with respect to the blank; therefore, the alkaloids could be classified as a mixed-type inhibitor.[42] Also, data in Table 2 showed that the presence of different alkaloidal concentration did not significantly change the cathodic Tafel slope, β_c relative to the blank. Hence, they were said to exert dominant anodic inhibition.[43] The results could be visualized from Fig. 6(d)–(f). The obtained R_p values showed a similar trend to that of R_{ct} in the impedance results where they appeared the highest at 1000 ppm. The corrosion current (i_{corr}) and potentials (E_{corr}) gradually decreased as the concentrations of the inhibitors increased. The protection actions of compound **1**, **2** and **3** were contributed from the electron density of the amine (–N–R_2), hydroxyl (–OH) and methoxyl groups (–OCH_3).[44] The nitrogen and oxygen atoms can donate their lone pair of electrons to the empty d-orbitals on the metal surface and forming a uniform layer of protection.[31] **2** showed 73.35% of IE% which was the highest among **1** and **3**. This is because **2** has the most protonatable functional groups and rigid molecular structures. The rigidity of the molecular structure of **2** ensures better orientation and adsorption of the inhibitor on the MS surface. The inhibitive action for these constituents increases in the following order: **1** < **3** < **2**. Hence, it is concluded that the chemical nature of the electrolyte affects the corrosion rate rather than the applied techniques.

Table 2 Polarization parameters for al the studied inhibitors on MS in 1 M HCl medium

Inhibitor	Conc. (ppm)	E_{corr} (mV)	i_{corr} (μA cm^{-2})	R_p (kΩ cm^2)	β_a (mV dec^{-1})	β_c (mV dec^{-1})	CR (m y^{-1})	IE (%)
—	0	−494	0.2594	72.20	77.8	96.8	3.07	—
CNHE	10	−489	0.2534	74.2	78.4	97.0	2.99	2.30
	100	−483	0.2390	87.5	95.4	97.4	2.82	7.86
	200	−477	0.2050	98.2	91.0	94.6	2.42	20.97
	500	−466	0.1863	114.3	96.7	99.6	2.20	28.16
	1000	−474	0.2058	104.8	95.0	104.3	2.43	20.64
CNDE	10	−454	0.1582	134.4	87.9	110.6	1.87	39.00
	100	−482	0.1008	210.5	104.9	91.5	1.19	61.13
	200	−480	0.0672	315.9	106.9	90.3	0.80	74.06
	500	−355	0.0450	485.5	113.3	90.6	0.53	**82.64**
	1000	−424	0.0544	395.7	108.3	91.4	0.64	79.03
CNME	10	−476	0.2079	94.7	74.8	115.2	2.45	19.85
	100	−453	0.1047	193.4	90.8	96.1	1.23	59.60
	200	−468	0.0851	243.8	93.8	97.5	1.00	67.18
	500	−456	0.0630	356.6	112.4	96.3	0.74	75.65
	1000	−435	0.0778	281.5	99.6	102.3	0.92	70.00
1	100	−479	0.1558	87.4	59.9	65.8	1.84	39.94
	200	−467	0.1080	124.9	60.8	63.6	1.27	58.34
	500	−456	0.0778	173.6	60.1	64.4	0.92	60.02
	1000	−458	0.0520	267.4	57.1	72.8	0.61	71.40
2	100	−465	0.2198	81.8	80.2	85.6	2.60	15.26
	200	−457	0.1806	105.0	86.8	87.9	2.13	30.37
	500	−472	0.0982	186.7	75.7	95.6	1.16	62.12
	1000	−435	0.0692	317.7	100.6	101.7	0.81	**73.35**
3	100	−473	0.2152	71.86	64.1	80.2	2.54	17.10
	200	−467	0.2200	119.5	65.5	805	2.60	15.15
	500	−455	0.1010	192.5	93.2	86.3	1.20	61.03
	1000	−462	0.0741	262.7	95.7	84.5	0.87	69.50

Open Access Article. Published on 12 February 2020. Downloaded on 1/23/2026 3:02:15 PM.
This article is licensed under a Creative Commons Attribution-NonCommercial 3.0 Unported Licence.

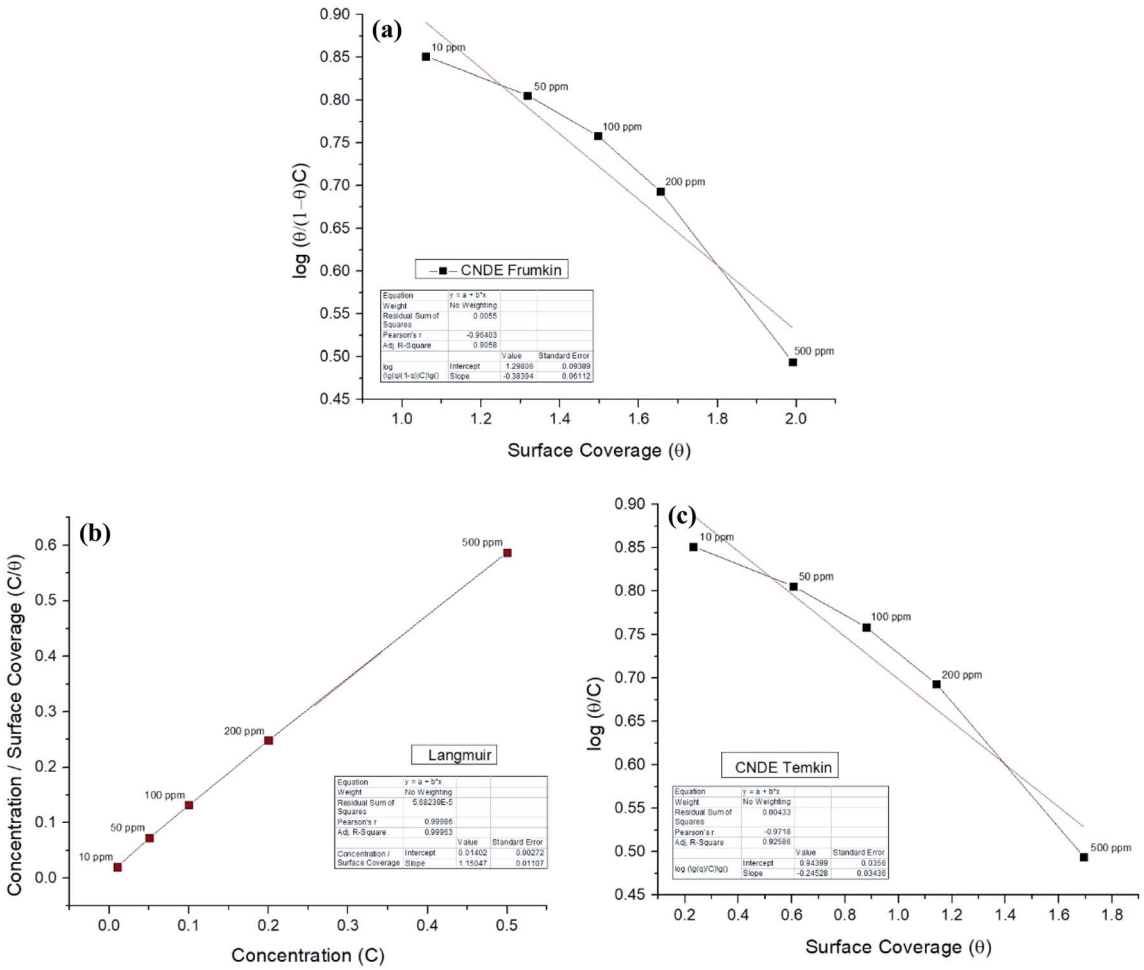

Fig. 7 (a) Frumkin, (b) Langmuir, (c) Temkin adsorption isotherm for all concentrations of CNDE on MS in 1 M HCl at 303 K.

3.3 Adsorption isotherm

Corrosion inhibition of mild steel is an exothermic process based on the dependence of ΔG_{ads} on temperature where increasing reaction temperature will cause desorption of inhibitor from the steel surface.[45] Two adsorption modes are commonly discussed in view of corrosion inhibition which are the chemisorption and physisorption.[46] Generally, physisorption is the electrostatic interaction between the charged molecules (counter ions) against the charged metal surface. Values of ΔG^0_{ads} until -20 kJ mol^{-1} are consistent with the physical adsorption while those lower than -40 kJ mol^{-1} are correlated with the chemisorption.[46,47] The nonbonding electron pairs at the electronegative sites may interact with the vacant d-orbitals of mild steel to provide a protective chemisorbed film.[48] In the case of the extracts, the absolute values are relatively higher compared to each of the alkaloids, approaching to those of chemisorption.

The inhibitive action of *Cryptocarya nigra* extracts towards acid corrosion of mild steel was discussed through Langmuir adsorption isotherm. CNDE best fitted the plot, having a linearity of R^2 value approximately 0.9997. The strength and stability of the adsorbed layer formed by CNDE could also be evaluated from the higher K_{ads} value as compared to the other extracts. The negative values of ΔG_{ads} ensure the stability and spontaneity of the adsorbed layer on the electrode surface.[49] ΔG_{ads} values calculated from the adsorption process was -28.2 kJ mol^{-1} which signified that the molecules were adsorbed on the steel surface through comprehensive physisorption and chemisorption interaction.[50] A comparison between different adsorption isotherm plots for CNDE were extrapolated in Fig. 7(a)–(c). The results are tabulated Table 3.

Table 3 Langmuir adsorption isotherm parameters for CNDE and three pure alkaloids

	CNDE	1	2	3
R^2	0.9997	0.9991	0.9952	0.9991
y-Intercept	0.0399	0.0484	0.0703	0.2909
K_{ads} value	25.0627	20.6612	14.2248	3.4376
ΔG_{ads} (J mol^{-1})	−28 232.95	−17 746.44	−16 806.12	−13 228.41

 This journal is © The Royal Society of Chemistry 2020

Open Access Article. Published on 12 February 2020. Downloaded on 1/23/2026 3:02:15 PM.
This article is licensed under a Creative Commons Attribution-NonCommercial 3.0 Unported Licence.

Thermodynamic parameters of the adsorption process were calculated, and all the three alkaloids were found out to be spontaneously adsorbed onto the MS through physisorption where their calculated ΔG were more than -20 kJ mol^{-1} as tabulated in Table 3. The ΔG values indicated that the alkaloids adsorbed on the MS surface through dominantly physisorption mechanism.[51] The alkaloids were protonated by the acidic media prior to forming an electrostatic interaction with the metal surface to prevent oxidation of Fe. The results obtained from the fitting on Langmuir plot in Fig. 8(a)–(c) showed good agreement with the results from the electrochemical method, where **2** provides better protection for mild steel against pitting corrosion in 1 M HCl solution having the highest R^2 value of 0.9998. The higher value of K_{ads} shows that the inhibitor adsorbed strongly on MS surface.[52,53] The IE% of these compounds are directly proportionated to their concentration and molecular weights.

3.4 Proposed mechanism of inhibition

CNDE consists of variety of constituents therefore, it displayed a higher ΔG_{ads} value indicating that the inhibition mechanism proceeds towards chemisorption. This mode of adsorption is the result of donor–acceptor interaction between the free electron pairs of heteroatoms and π electrons of multiple bonds from the combination of constituents with the vacant d-orbitals of iron.[23] The synergistic effect resulted from the multiple components formed a better and stronger interaction of adsorption on the surface of the mild steel.

The inhibition mechanism of the pure alkaloids is dependent on their total molecular structures and the spatial relationship of different functional groups. The more electron donor groups introduced, particularly substituents with conjugated systems will improve corrosion inhibition efficiency of inhibitor derivatives.[35,54]

When these structures are incorporated with multiple fused aromatic or aliphatic rings, additional substituents such as protonatable amine or hydroxyl groups may improve their solubilities in the aqueous corrosive fluid. If nitrogen is protonated, the counter anion, Cl^- will enhance the adsorption of compounds.[73] Linked quaternary nitrogen-containing groups can be more effective as corrosion inhibitors than a molecule containing a single such group. A linking group containing carbon and hydrogen atoms can serve to make the molecule

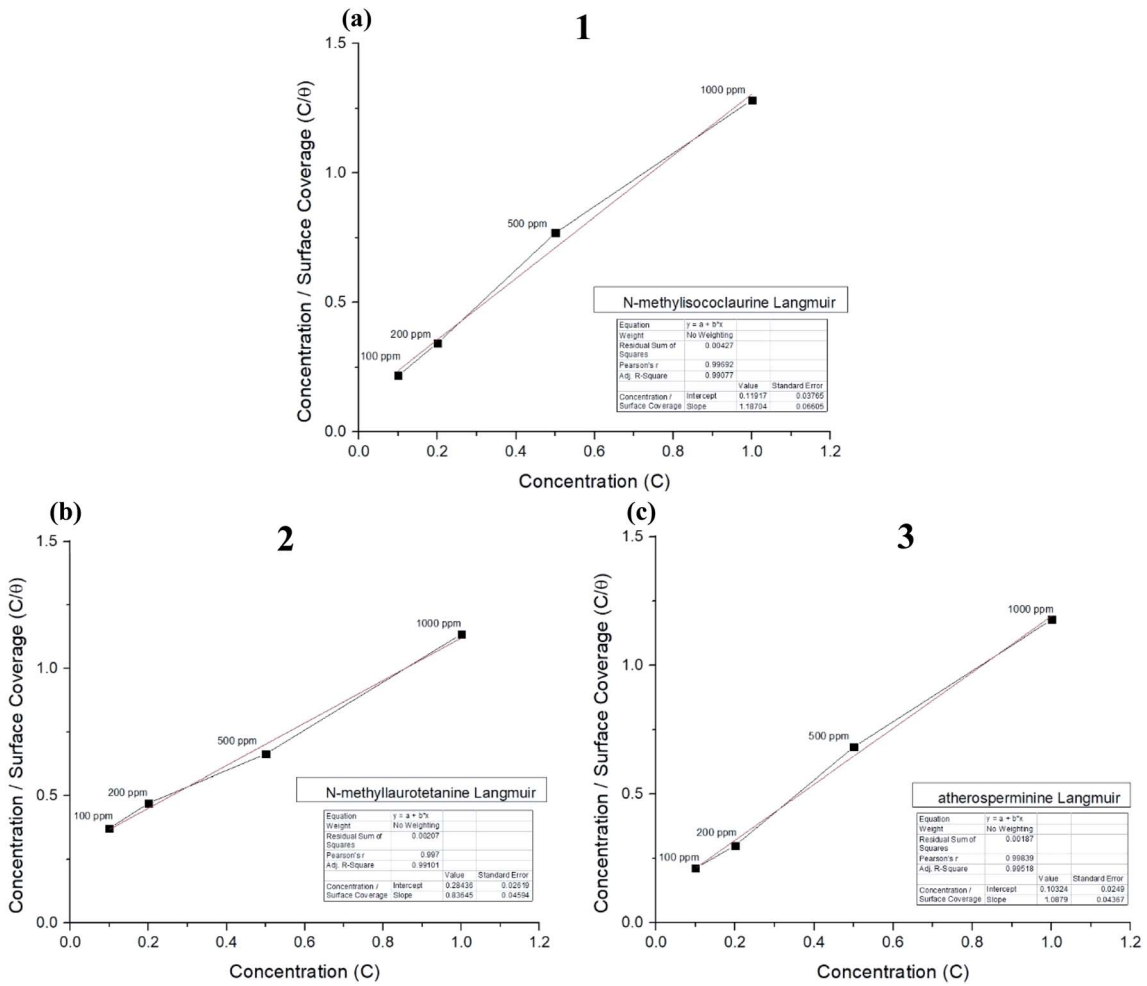

Fig. 8 Langmuir adsorption plots for (a) *N*-methylisococlaurine **1**, (b) *N*-methyllaurotetanine **2** and (c) atherosperminine **3**, respectively.

Open Access Article. Published on 12 February 2020. Downloaded on 1/23/2026 3:02:15 PM.
This article is licensed under a Creative Commons Attribution-NonCommercial 3.0 Unported Licence.

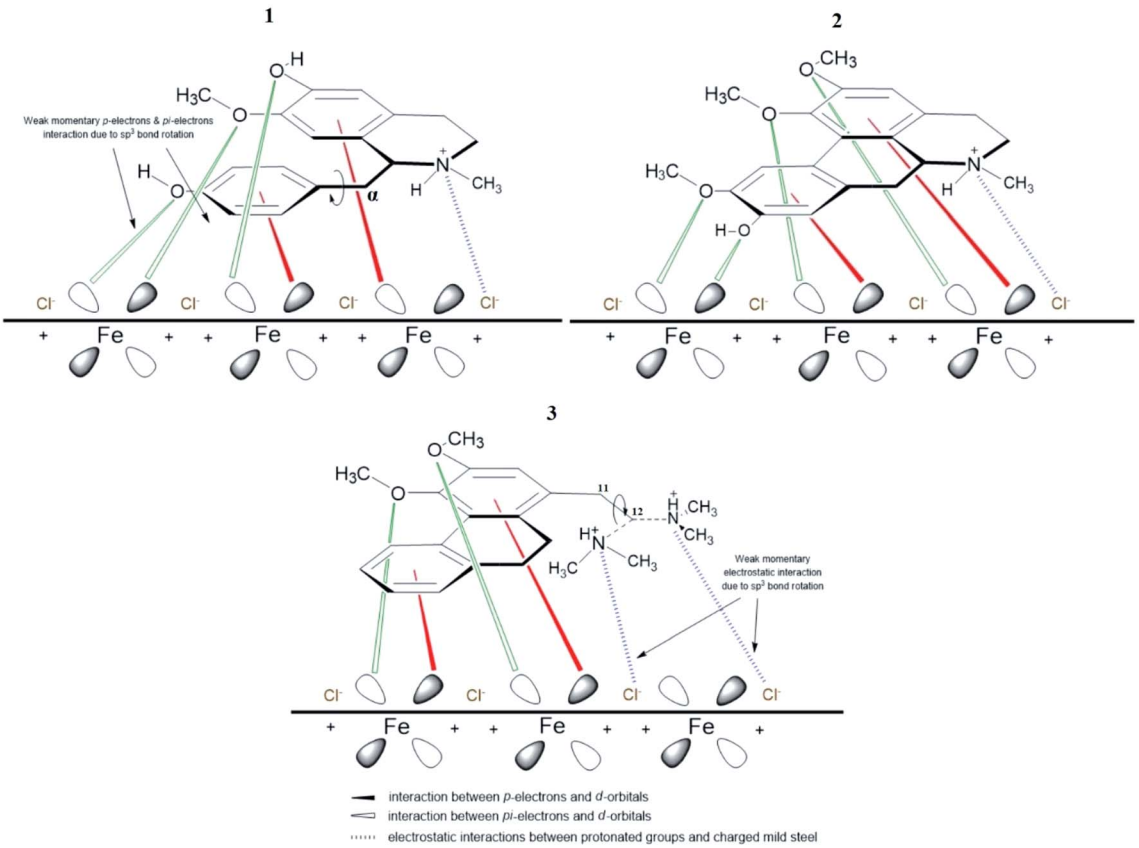

Fig. 9 Different spatial adsorption interactions of 1, 2 and 3.

more hydrophobic, which can also enhance effectiveness as a corrosion inhibitor.[44,55]

In the case of the studied alkaloids, the inhibition effects of the respective compound were governed by the interaction between π electrons of phenyl rings and p-electrons from the electron donor groups (N and O) with the vacant d-orbitals of iron through which they form insoluble, stable and uniform thin film on MS surface.[44,56] The results shown by EIS, PDP and adsorption isotherm fitting clearly deduced that the inhibition mechanism for all studied inhibitors involves blocking of mild steel surface *via* adsorption at the metal-solution interface.[57] The adsorption of inhibitors was influenced by the nature, temperature and morphology of the metal as well as the chemical structure of the inhibitors.[1,2] The values of IE% depend essentially on the electron density at the active centre(s) of the inhibitor molecule. The thermodynamic parameters in Table 3 prove that the adsorption of alkaloids on the MS surface in 1 M HCl are more towards physisorption than

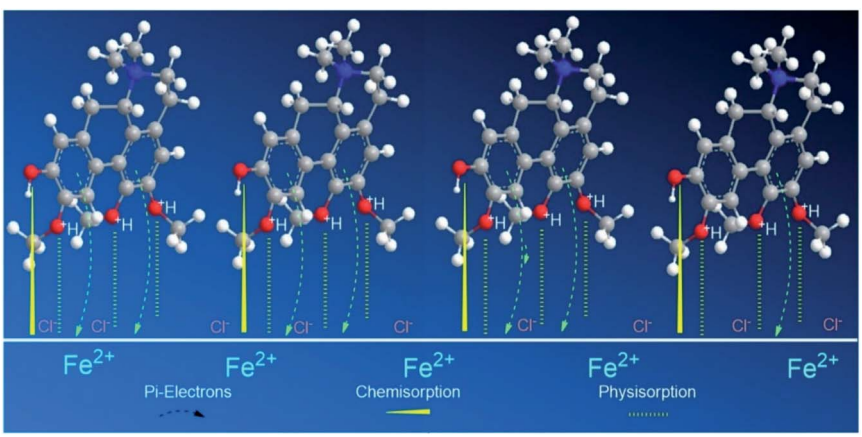

Fig. 10 Staggered and systematic arrangement of 2 on the MS surface.

 This journal is © The Royal Society of Chemistry 2020

Open Access Article. Published on 12 February 2020. Downloaded on 1/23/2026 3:02:15 PM.
This article is licensed under a Creative Commons Attribution-NonCommercial 3.0 Unported Licence.

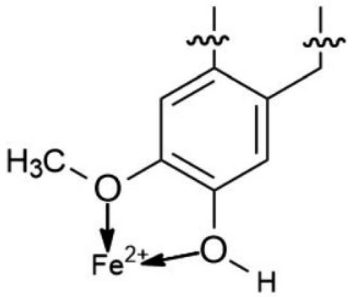

Fig. 11 Structural representation of Fe^{2+}-2 complex.

chemisorption. The physisorption of these alkaloids arise from the electrostatic interaction between the protonated electronegative sites and the charged surface of iron(II) chloride, $(FeCl^{-})_{ads}$.[58]

The different spatial adsorption interactions of **1**, **3** and **2** on mild steel surface are illustrated in Fig. 9 below. For alkaloid **1**, a phenyl ring is interconnected with the isoquinoline moiety through the α-carbon which is sp^3 hybridized and can freely rotate. This free bond rotation causes a weak momentary interaction of π- and nonbonding lone pair electrons of oxygen on the phenyl ring with the vacant d-orbitals of iron,[59–62] consequently resulting in a lower IE%. For alkaloid **3**, an *N*,*N*-dimethylethylamine group is attached to the phenanthrene moiety and the carbon at position 11 and 12 are sp^3 hybridized. The link between these two carbons are free to rotate, hence inducing rotation of the amino group. This eventually leads to a weak momentary electrostatic interaction between the protonated amino group and $(FeCl^{-})_{ads}$ species on the mild steel surface,[44,63] thus leading to a lower IE% value.

However, for alkaloid **2**, the three methoxyl and 1 hydroxyl groups on the aporphine structure are aligned in the same direction. As a result, forming the highest electron density over a specific area. The arrangements of the functional groups in a rigid structure aids the effectiveness of the adsorption process of **2** on mild steel surface. Aromatic compounds with cyclic delocalized π-electron system are susceptible to electron delocalization in acidic media.[35,64] The importance of the planarity shape of the benzene ring is described by the orbital approach. Owing to the trigonal planar shape of carbons having sp^2 hybridized orbitals, the rings of **2** are flat and there is no possibility for free rotation of bond to occur.[65] This flatness property permits the overlapping of the p-orbitals in both directions indirectly forming a stable monolayer of protection.[66] Formation of a smooth homogenous monolayer by **2** on the MS surface has led to higher surface coverage, Θ (Fig. 10) thus making the IE% of the alkaloid the highest as compared to the other two.[67]

The proposed formation of Fe^{2+}-**3** complex is accomplished by a coordinative bond from the nonbonding lone pair electrons on the oxygen atom towards the Fe^{2+} as shown in Fig. 11. The deprotonation of hydroxyl group by the existing Cl^{-} species present in the 1 M HCl media causes a resonance effect onto the aromatic ring.[68,69] This effect is generated due to substituents on the ring that causes the delocalization of π-electrons. The stabilization of the π-electrons creates an excess positive charge on the oxygen atom of the adjacent *ortho*-located methoxyl group (Fig. 12).[70]

3.5 Surface analysis

The surface morphology of MS due to corrosion process was examined under SEM analysis along with EDX to determine the elemental compositions on the surface before and after the exposure to the corrosive media with and without the inhibitors.[71,72] Fig. 13(a)–(d) displays an array of the SEM-EDX micrographs recorded for (a) polished mild steel, (b) without any inhibitors, (c) with the presence of 1000 ppm CNDE, and (d) with the presence of 1000 ppm **2**. No sign of corrosion action has taken place on the polished mild steel surface looking from Fig. 13(a).[70]

Fig. 13(b) revealed that without any inhibitive actions the surface of MS appeared to be highly corroded with areas of localized corrosion. However, in the presence of 500 ppm CNDE in Fig. 13(c) the corrosion activity was suppressed as seen from the decrease in localized corrosion areas. This is due to the adsorption of inhibitors on the mild steel surface forming a monolayer of protection against corrosion activity.[73]

In Table 4, elemental analysis of corroded sample, Fig. 13(b) using energy dispersive X-ray spectroscopy (EDX) revealed the percentage of chlorine (Cl) and oxygen (O) are immense due to the formation of adsorptive ferrous chloride $(FeCl)_{ads}$ which can further oxidize to form ferric hydroxide $(Fe(OH)_3)$ and oxyhydroxides (FeOOH).[74] In the case of MS immersed in 1 M HCl with CNDE inhibitor, only trace amount of Cl^{-} and O were

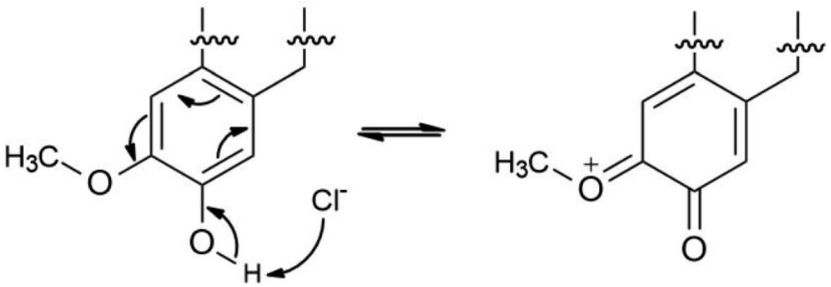

Fig. 12 Electron delocalization on compound **2** due to resonance effect.

Open Access Article. Published on 12 February 2020. Downloaded on 1/23/2026 3:02:15 PM.
This article is licensed under a Creative Commons Attribution-NonCommercial 3.0 Unported Licence.

detected indicating that the corrosion process has been inhibited significantly.[75] The presence of CNDE as corrosion inhibitors has decreased the oxygen reduction process hence reducing the corrosion rate. The decreased in oxygen value shows effectiveness of this inhibitor.

2 exhibited positive impact in preventing the corrosion on mild steel as shown in SEM micrograph displayed in Fig. 13(d). The percentage of Fe is higher than that of the corroded sample with only less than 10% of oxygen and chlorine elements. Excess negative charge resulted from the adsorption of Cl^- promotes

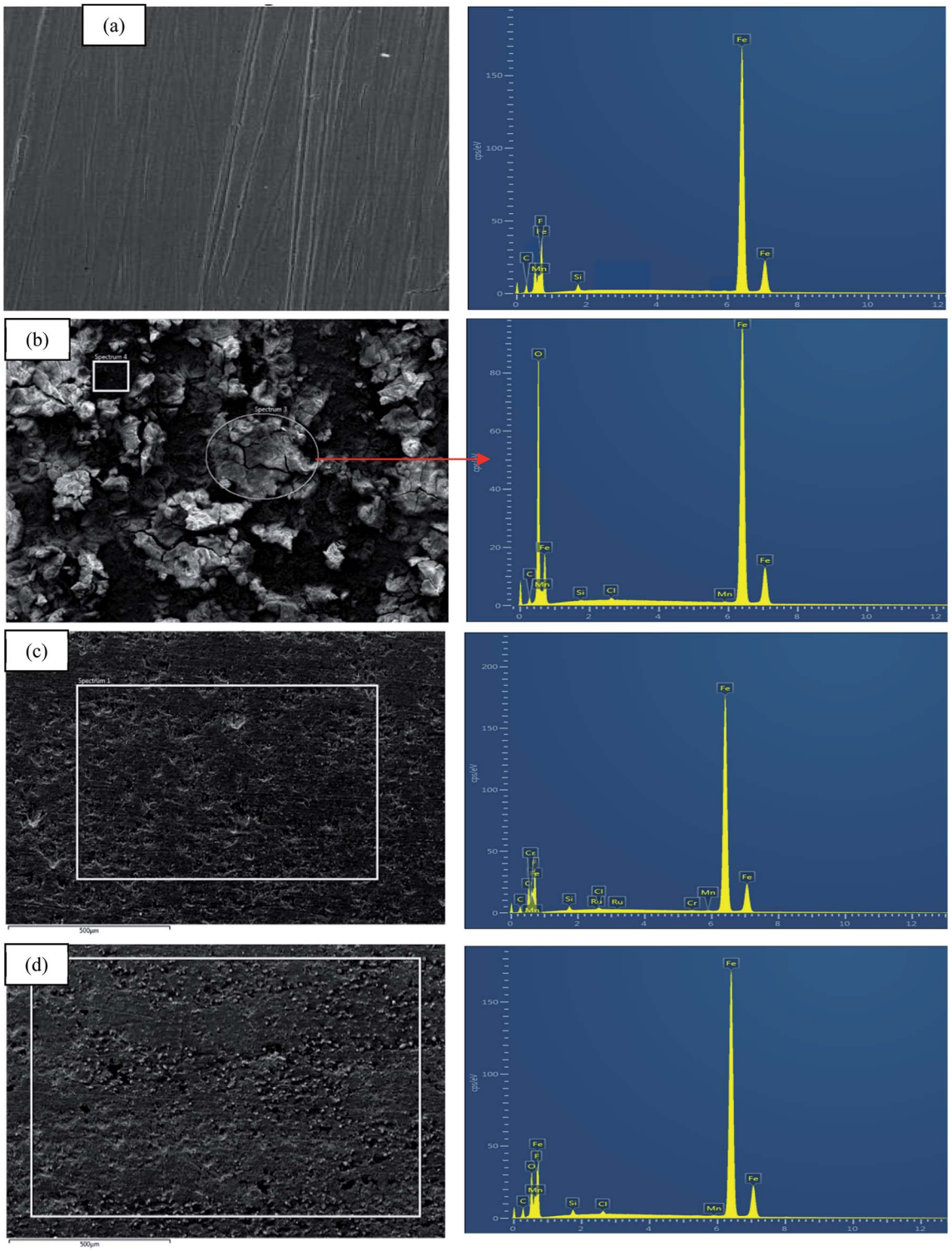

Fig. 13 SEM micrographs for (a) polished MS, (b) corroded MS, (c) MS with the presence of 500 CNDE, (d) with the presence of 1000 ppm **2**. All at the magnification of 500×.

 This journal is © The Royal Society of Chemistry 2020

Open Access Article. Published on 12 February 2020. Downloaded on 1/23/2026 3:02:15 PM.
This article is licensed under a Creative Commons Attribution-NonCommercial 3.0 Unported Licence.

Table 4 The percentage of elements for each specimen obtained from the energy dispersive X-ray spectroscopy (EDX) analysis after 24 h immersion in 1 M HCl

Sample	Element (% wt)			
	Fe	O	C	Cl
(a) Untreated polished mild steel	99.4	—	0.13	—
(b) Mild steel in 1 M HCl	50.5	41.7	3.2	2.7
(c) Mild steel in 500 ppm CNDE	82.8	10.2	5.1	1.2
(d) Mild steel in 1000 ppm **2**	76.2	16.6	6.3	1.5

Table 5 The wastewater parameters of four different samples; **1**, **2** and **3**

	CNDE	1	2	3
pH	6.7	7.2	6.9	7.4
COD_{Cr} (after 5 hours)	70.5	30.9	33.8	25.0
BOD_5 (after 5 days)	10.9	11.2	8.4	7.7
BOD_5/COD_{Cr}	0.15	0.36	0.24	0.31
Zinc	0.02	0.01	na	na
Free Cl	0.01	na	na	0.01
Turbidity (NTU)	0.2	0.2	0.1	0.2

electrostatic interaction with cations (protonated alkaloids).[76] The protonated inhibitor molecules will adsorb on the mild steel surface *via* chloride ions which form an interconnecting bridge upon replacement of chloride and water molecules.[77] Electrostatic interaction was believed to be generated between the protonated molecules and $(FeCl^-)_{ads}$ species at anodic sites.[78,79] Surface analysis using scanning electron microscope (SEM) proved a significant improvement on the morphology of the mild steel plates in the presence of an optimum concentration of CNDE and **2** inhibitors.

3.6 Water quality test

When waste-water including urban runoff is discharged into a watercourse, it exerts a polluting load on that water body. Micro-organisms present in the natural water and the waste-water break down the organic matter. As the early forms of wastewater treatment developed are aerobic, the simplest way of measuring the biodegradability of the wastewater is to estimate the amount of oxygen required to breakdown the waste.[80] This type of system is known as the biochemical oxygen demand (BOD) test. Traditionally, the BOD test is carried out for five days and the resulting oxygen demand is referred to as BOD_5. In practice, the test is often modified slightly in that a number of seed micro-organisms are added to the BOD bottle to overcome the initial lag period. In chemical oxygen demand (COD) methodology, strong chemical reagents are used to oxidize the waste. The COD test oxidizes material within shorter period of hours that micro-organisms cannot metabolize in five days. Most wastewater treatment processes operate best in pH ranges between 6.8 and 7.4 (Fig. 14).

The physico-chemical analysis of the wastewater developed from the addition of the pure compounds was tabulated in Table 5. Based on the results shown in Table 5, the pure compounds values were within the permissible limits to discharge for irrigation and horticultural uses. According to Central Pollution Control Board (CPCB), the permissible limits of COD and BOD concentrations are 250 mg L^{-1} and 30 mg L^{-1}, respectively.[81]

The value of BOD_5/COD_{Cr} is commonly adopted to evaluate biodegrading property of wastewater, although the value is not always in agreement with the biodegradability in some special situations. However, it is a good surface indication of whether a particular substance could be easily decomposed in a given water sample by the natural microorganism. In general, a higher BOD_5/COD_{Cr} value of a wastewater implies a higher degree of biodegradability. When the value is lower than 0.20, the wastewater is usually considered hardly biodegradable. From this point of view, it could be deduced that the pure compounds' whose values are between the range of 0.24–0.36 (Table 5), are moderately easy to be biodegraded. To date, many

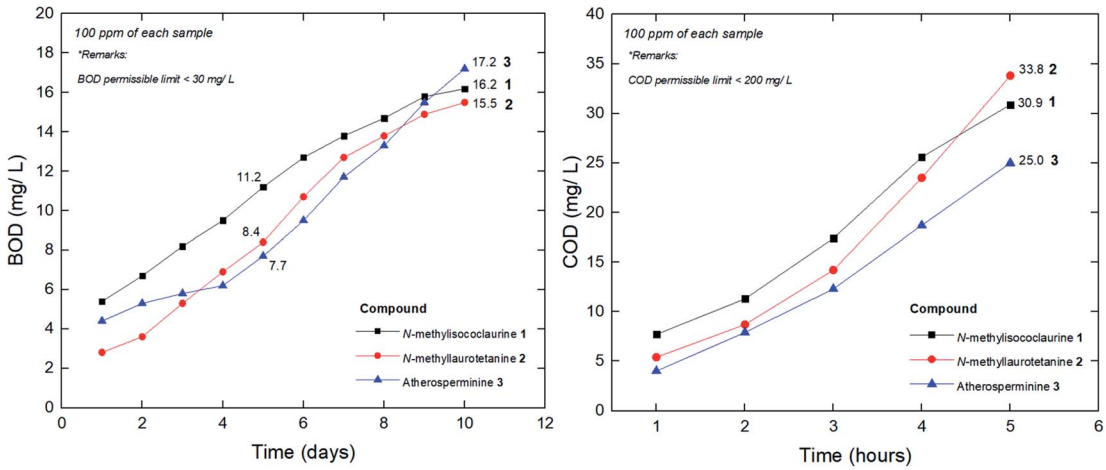

Fig. 14 BOD and COD curves for the pure compounds isolated from CNDE.

Open Access Article. Published on 12 February 2020. Downloaded on 1/23/2026 3:02:15 PM.
This article is licensed under a Creative Commons Attribution-NonCommercial 3.0 Unported Licence.

technologies have been explored to develop efficient treating methods for the wastewater. There are quite a number of publications that have reported on the COD and BOD reduction through several technological approaches derived from natural plant components as a substitute for activated carbon filter. The innovation involved the implementation of fruit peels,[82] biofilm,[83] tannin-based coagulant, activated sludge,[84] electrochemical processes,[85] microphyte system,[86] microbial fuel cell,[87] advanced oxidation and ultrafiltration.[88]

4. Conclusions

This study presented that *Cryptocarya nigra* dichloromethane extract (CNDE) has potent corrosion inhibition action on mild steel in 1 M HCl media and alkaloid **2** showed the highest inhibitory activity amongst all the alkaloids studied. These alkaloids behaved as good corrosion inhibitors due to the presence of nitrogen (N) as the base element in the vicinity of their structure, with **2** possesses the most oxygenated functional groups and rigid structure as compared to the other alkaloids. The theoretical prediction is supported by the retrieved experimental results in the following order: **2** > **3** > **1**. They also exhibited COD and BOD values that are within permissible limits set by CPCB. In a nutshell, the results attained have proven that alkaloids can be good potential candidates as green corrosion inhibitors.

Conflicts of interest

There are no conflicts to declare.

Acknowledgements

The authors would like to express our gratifications to University Malaya Research Grant (Bantuan Kecil Penyelidikan, BKP), (BK040-2017) and RU Grant under Faculty Program (GPF052B-2018) as this work would not have been successful without the financial support given. We also acknowledge the help given by Din Mohd Nor, Hasri Abdullah and Rafly Syamsir from the Herbarium Group, University of Malaya and Teo Leong Eng for the plant collection and identification. This work was carried out in the framework of the International French Malaysian Natural Product Laboratory (IFM-NatPro-Lab). Special recognitions are dedicated to University Science Malaysia (USM), Penang for the determination of anti-corrosion activities.

References

1 C. Verma, E. E. Ebenso and M. A. Quraishi, *J. Mol. Liq.*, 2017, **233**, 403–414.
2 C. Verma, E. E. Ebenso, I. Bahadur and M. A. Quraishi, *J. Mol. Liq.*, 2018, **266**, 577–590.
3 S. A. Umoren, M. M. Solomon, I. B. Obot and R. K. Sulieman, *J. Ind. Eng. Chem.*, 2019, **76**, 91–115.
4 A. B. Hamdan and F. I. Haider, *IOP Conf. Ser. Mater. Sci. Eng.*, 2018, **290**, 12–86.
5 E. E. Oguzie, *Corros. Sci.*, 2008, **50**(11), 2993–2998.
6 G. Ji, S. Anjum, S. Sundaram and R. Prakash, *Corros. Sci.*, 2015, **90**, 107–117.
7 A. K. Satapathy, G. Gunasekaran, S. C. Sahoo, K. Amit and P. V. Rodrigues, *Corros. Sci.*, 2009, **51**(12), 2848–2856.
8 M. H. Hussin and M. J. Kassim, *Mater. Chem. Phys.*, 2011, **125**(3), 461–468.
9 P. E. Alvarez, M. V. Fiori-Bimbi, A. Neske, S. A. Brandán and C. A. Gervasi, *J. Ind. Eng. Chem.*, 2018, **58**, 92–99.
10 E. Alibakhshi, M. Ramezanzadeh, G. Bahlakeh, B. Ramezanzadeh, M. Mahdavian and M. Motamedi, *J. Mol. Liq.*, 2018, **255**, 185–198.
11 R. Haldhar, D. Prasad and N. Bhardwaj, *J. Adhes. Sci. Technol.*, 2019, **33**(11), 1169–1183.
12 P. B. Raja, A. K. Qureshi, A. Abdul Rahim, H. Osman and K. Awang, *Corros. Sci.*, 2013, **69**, 292–301.
13 A. A. Rahim, M. J. Kassim, E. Rocca and J. Steinmetz, *Corros. Eng., Sci. Technol.*, 2011, **46**(4), 425–431.
14 M. Chigondo and F. Chigondo, *J. Chem.*, 2016, 7.
15 B. Ngouné, M. Pengou, A. M. Nouteza, C. P. Nanseu-Njiki and E. Ngameni, *ACS Omega*, 2019, **4**(5), 9081–9091.
16 P. B. Raja, M. Fadaeinasab, A. K. Qureshi, A. A. Rahim, H. Osman, M. Litaudon and K. Awang, *Ind. Eng. Chem. Res.*, 2013, **52**(31), 10582–10593.
17 L. G. Saw and R. C. K. Chung, *Rodriguesia*, 2015, **66**(4), 947–960.
18 A. A. Nasrullah, Doctoral dissertation, Jabatan Kimia, Fakulti Sains, Universiti Malaya, 2014.
19 D. L. Custodio and V. F. da V. Junior, *RSC Adv.*, 2014, **4**(42), 21864–21890.
20 W. N. N. Wan Othman, Y. Sivasothy, S. Y. Liew, J. Mohamad, M. A. Nafiah, K. Ahmad, K. Awang, *et al.*, *Phytochem. Lett.*, 2017, **21**, 230–236.
21 S. M. Abd El Haleem, S. Abd El Wanees, E. E. Abd El Aal and A. Farouk, *Corros. Sci.*, 2013, **68**, 1–13.
22 M. M. Aslam, M. A. Baig, I. Hassan, I. A. Qazi, M. Malik and H. Saeed, *Electron. J. Environ., Agric. Food Chem.*, 2004, **3**(6), 804–811.
23 S. K. Saha, A. Dutta, P. Ghosh, D. Sukul and P. Banerjee, *Phys. Chem. Chem. Phys.*, 2016, **18**(27), 17898–17911.
24 A. Nasrullah, A. Zahari, J. Mohamad and K. Awang, *Molecules*, 2013, **18**(7), 8009–8017.
25 J. Kunitomo, Y. Yoshikawa, S. Tanaka, Y. Imori, K. Isoi, Y. Masada and T. Inoue, *Phytochemistry*, 1973, **12**(3), 699–701.
26 S. S. Lee, Y. C. Lai, C. K. Chen, L. H. Tseng and C. Y. Wang, *J. Nat. Prod.*, 2007, **70**(4), 637–642.
27 A. Zahari, A. Ablat, Y. Sivasothy, J. Mohamad, M. I. Choudhary and K. Awang, *Asian Pac. J. Trop. Med.*, 2016, **9**(4), 328–332.
28 C. H. Lin, F. N. Ko, Y. C. Wu, S. T. Lu and C. M. Teng, *Eur. J. Pharmacol.*, 1993, **237**(1), 109–116.
29 K. Stanly Jacob and G. Parameswaran, *Corros. Sci.*, 2010, **52**(1), 224–228.
30 K. Juttner, *Electrochim. Acta*, 1990, **35**(10), 1501–1508.
31 M. H. Hussin, M. Jain Kassim, N. N. Razali, N. H. Dahon and D. Nasshorudin, *Arabian J. Chem.*, 2016, **9**, S616–S624.

 This journal is © The Royal Society of Chemistry 2020

Open Access Article. Published on 12 February 2020. Downloaded on 1/23/2026 3:02:15 PM.
This article is licensed under a Creative Commons Attribution-NonCommercial 3.0 Unported Licence.

32 A. Mathina and R. Rajalakshmi, *Rasayan J. Chem.*, 2016, **9**(1), 56–66.
33 A. K. Satapathy, G. Gunasekaran, S. C. Sahoo, K. Amit and P. V. Rodrigues, *Corros. Sci.*, 2009, **51**(12), 2848–2856.
34 R. G. Inzunza, B. V. Salas, M. S. Wiener, M. C. Beltran, R. Z. Koytchev, M. S. Stilianova, J. T. Gaynor, *et al.*, *Int. J. Electrochem. Sci.*, 2013, **8**(5), 6433–6448.
35 E. B. Barmatov, J. F. Geddes, L. P. Crawford, T. L. Hughes and N. V. Michaela, US Patent application no. 15/533,315, 2017.
36 M. A. Amin, K. F. Khaled, Q. Mohsen and H. A. Arida, *Corros. Sci.*, 2010, **52**(5), 1684–1695.
37 S. K. Sharma and A. Sharma, in *Green corrosion chemistry and engineering*, Wiley–VCH Publications, 2011, pp. 157–176.
38 H. Keleş, *Mater. Chem. Phys.*, 2011, **130**(3), 1317–1324.
39 R. Bandy, *Corros. Sci.*, 1980, **20**(8), 1017–1028.
40 R. Yıldız, A. Döner, T. Doğan and İ. Dehri, *Corros. Sci.*, 2014, **82**, 125–132.
41 A. Chetouani, B. Hammouti, T. Benhadda and M. Daoudi, *Appl. Surf. Sci.*, 2005, **249**(1), 375–385.
42 A. Chetouani, K. Medjahed, K. E. Sid-Lakhdar, B. Hammouti, M. Benkaddour and A. Mansri, *Corros. Sci.*, 2004, **46**(10), 2421–2430.
43 M. Lagrenee, B. Mernari, M. Bouanis, M. Traisnel and F. Bentiss, *Corros. Sci.*, 2002, **44**(3), 573–588.
44 L. P. Crawford, E. B. Barmatov, T. L. Hughes and M. Y. Ho, *US Pat.*, 15/566,529, 2018.
45 A. Ostovari, S. M. Hoseinieh, M. Peikari, S. R. Shadizadeh and S. J. Hashemi, *Corros. Sci.*, 2009, **51**(9), 1935–1949.
46 C. Lai, B. Xie, L. Zou, X. Zheng, X. Ma and S. Zhu, *Results Phys.*, 2017, **7**, 3434–3443.
47 A. Mohammadi, S. M. A. Hosseini, M. J. Bahrami and M. Shahidi, *Prog. Color, Color. Coat.*, 2016, **9**(2), 117–134.
48 M. Gobara, B. Zaghloul, A. Baraka, M. Elsayed, M. Zorainy, M. M. Kotb and H. Elnabarawy, *Mater. Res. Express*, 2017, **4**(4), 046504.
49 L. O. Olasunkanmi, I. B. Obot, M. M. Kabanda and E. E. Ebenso, *J. Phys. Chem. C*, 2015, **119**(28), 16004–16019.
50 J. Yamuna and N. Anthony, *Int. J. ChemTech Res.*, 2015, **7**(1), 37–43.
51 A. Singh, I. Ahamad, V. K. Singh and M. A. Quraishi, *J. Solid State Electrochem.*, 2011, **15**(6), 1087–1097.
52 A. Chetouani, B. Hammouti, T. Benhadda and M. Daoudi, *Appl. Surf. Sci.*, 2005, **249**(1), 375–385.
53 M. H. Hussin, A. A. Rahim, M. N. Mohamad Ibrahim and N. Brosse, *Ind. Crop. Prod.*, 2013, **49**, 23–32.
54 D. Daoud, T. Douadi, H. Hamani, S. Chafaa and M. Al-Noaimi, *Corros. Sci.*, 2015, **94**, 21–37.
55 M. R. Vinutha and T. V. Venkatesha, *Port. Electrochim. Acta*, 2016, **34**(3), 157–184.
56 K. Barouni, L. Bazzi, R. Salghi, M. Mihit, B. Hammouti, A. Albourine and S. El Issami, *Mater. Lett.*, 2008, **62**(19), 3325–3327.
57 P. B. Raja, A. A. Rahim, H. Osman and K. Awang, *ActaPhys. Chim. Sin.*, 2010, **26**, 2171–2176.
58 M. Ramdani, H. Elmsellem, B. Haloui, N. Elkhiati, M. Layachi, A. Mesfioui, B. El Mahi, *et al.*, *Pharma Chem.*, 2016, **8**(1), 330–337.
59 B. D. Burkitbayeva, A. M. Argimbayeva, G. S. Rakhymbay, G. S. Beisenova and K. Avchukir, *Int. J. Biol. Chem.*, 2016, **9**(1), 83–94.
60 Z. Cao, Y. Tang, H. Cang, J. Xu, G. Lu and W. Jing, *Corros. Sci.*, 2014, **83**, 292–298.
61 P. Singh, E. E. Ebenso, L. O. Olasunkanmi, I. B. Obot and M. A. Quraishi, *J. Phys. Chem. C*, 2016, **120**(6), 3408–3419.
62 A. Kosari, M. H. Moayed, A. Davoodi, R. Parvizi, M. Momeni, H. Eshghi and H. Moradi, *Corros. Sci.*, 2014, **78**, 138–150.
63 M. P. Chakravarthy and K. N. Mohana, *ISRN Corrosion*, 2014.
64 J. Dokic, M. Gothe, J. Wirth, M. V. Peters, J. Schwarz, S. Hecht and P. Saalfrank, *J. Phys. Chem. A*, 2009, **113**(24), 6763–6773.
65 P. C. Okafor, M. E. Ikpi, I. E. Uwah, E. E. Ebenso, U. J. Ekpe and S. A. Umoren, *Corros. Sci.*, 2008, **50**(8), 2310–2317.
66 Z. Sanaei, M. Ramezanzadeh, G. Bahlakeh and B. Ramezanzadeh, *J. Ind. Eng. Chem.*, 2019, **69**, 18–31.
67 K. O. Sulaiman, A. T. Onawole, O. Faye and D. T. Shuaib, *J. Mol. Liq.*, 2019, **279**, 342–350.
68 B. Xu, Y. Liu, X. Yin, W. Yang and Y. Chen, *Corros. Sci.*, 2013, **74**, 206–213.
69 H. M. Abd El-Lateef, *Corros. Sci.*, 2015, **92**, 104–117.
70 M. Murmu, S. K. Saha, N. C. Murmu and P. Banerjee, *Corros. Sci.*, 2019, **146**, 134–151.
71 E. E. Ebenso, K. F. Khaled, S. K. Shukla, A. K. Singh, N. O. Eddy, M. Saracoglu, M. M. Kabanda, *et al.*, *Int. J. Electrochem. Sci.*, 2012, **7**, 5643–5676.
72 N. V. Likhanova, N. Nava, O. Olivares-Xometl, M. A. Domínguez-Aguilar, P. Arellanes-Lozada, I. V. Lijanova and L. Lartundo-Rojas, *Int. J. Electrochem. Sci.*, 2018, **13**, 7949–7967.
73 N. Asadi, M. Ramezanzadeh, G. Bahlakeh and B. Ramezanzadeh, *J. Taiwan Inst. Chem. Eng.*, 2019, **95**, 252–272.
74 S. Marzorati, L. Verotta and P. S. Trasatti, *Molecules*, 2018, **24**, 48.
75 N. A. Odewunmi, S. A. Umoren, Z. M. Gasem, S. A. Ganiyu and Q. Muhammad, *J. Taiwan Inst. Chem. Eng.*, 2015, **51**, 177–185.
76 Z. Sanaei, M. Ramezanzadeh, G. Bahlakeh and B. Ramezanzadeh, *J. Taiwan Inst. Chem. Eng.*, 2019, **69**, 18–31.
77 M. Benarioua, A. Mihi, N. Bouzeghaia and M. Naoun, *Egypt. J. Pet.*, 2019, **28**(2), 155–159.
78 C. Chai, Y. Xu, D. Li, X. Zhao, Y. Xu, L. Zhang and Y. Wu, *Prog. Org. Coating*, 2019, **129**, 159–170.
79 X. Luo, C. Ci, J. Li, K. Lin, S. Du and H. Zhang, *Corros. Sci.*, 2019, **151**, 132–142.
80 G. Ansola, C. Fernandez and E. De Luis, *Ecol. Eng.*, 1995, **5**(1), 13–19.
81 S. A. Paul, S. K. Chavan and S. D. Khambe, *Int. J. Chem.*, 2012, **10**(2), 635–642.
82 L. Li, S. Zhang, G. Li and H. Zhao, *Anal. Chim. Acta*, 2012, **754**, 47–53.

Open Access Article. Published on 12 February 2020. Downloaded on 1/23/2026 3:02:15 PM.
This article is licensed under a Creative Commons Attribution-NonCommercial 3.0 Unported Licence.

83 Q. He, K. Yao, D. Sun and B. Shi, *Biodegradation*, 2007, **18**(4), 465–472.
84 J. Sánchez-Martín, J. Beltrán-Heredia and C. Solera-Hernández, *J. Environ. Manage.*, 2010, **91**(10), 2051–2058.
85 S. A. Al-Jalil, *Biotechnology*, 2009, **8**(4), 473–477.
86 M. H. Hu, Y. S. Ao, X. E. Yang and T. Q. Li, *Agric. Water Manag.*, 2008, **95**(5), 607–615.
87 L. Huang, S. Cheng, F. Rezaei and B. E. Logan, *Environ. Technol.*, 2009, **30**(5), 499–504.
88 X. Dai, J. Fang, L. Li, Y. Dong and J. Zhang, *Int. J. Environ. Res. Public Health*, 2019, **16**(17), 3223.

 This journal is © The Royal Society of Chemistry 2020